Electronic structure of $Ga_{1-x}Mn_xAs$ analyzed according to hole-concentration-dependent measurements

M. A. Mayer,[1,2] P. R. Stone,[1,2] N. Miller,[1,2] H. M. Smith III,[1,2] O. D. Dubon,[1,2] E. E. Haller,[1,2] K. M. Yu,[1] W. Walukiewicz,[1] X. Liu,[3] and J. K. Furdyna[3]

[1]*Materials Sciences Division, Lawrence Berkeley National Laboratory, Berkeley, California 94720, USA*

[2]*Department of Materials Science and Engineering, University of California, Berkeley, California 94720, USA*

[3]*Department of Physics, University of Notre Dame, Notre Dame, Indiana 46556, USA*

(Received 18 November 2009; revised manuscript received 17 December 2009; published 22 January 2010)

We study the effects of variable hole concentration on the transport, thermoelectric, and magnetic properties of $Ga_{1-x}Mn_xAs$. The hole concentration in samples with fixed Mn content has been varied using high energy particle irradiation, which introduces donorlike defects that compensate Mn acceptors without changing the concentration of localized Mn spins. As expected, a decrease of the hole concentration results in a reduction of the Curie temperature and an increase in electrical resistivity and thermoelectric power. The mobility and thermopower data are then analyzed in terms of models based on free holes in the valence band and holes localized in a Mn impurity band. The energetic structure of the impurity band is described by the valence-band anticrossing model. We show that the electronic structure provided by the impurity band model is consistent with the experimental results.

DOI: 10.1103/PhysRevB.81.045205 PACS number(s): 71.20.Nr, 73.61.Ey, 72.20.Dp, 72.20.Pa

I. INTRODUCTION

Dilute magnetic semiconductors (DMSs) are regarded with high interest because of magnetic properties that can be probed or controlled electrically and alternatively electronic properties that are influenced by magnetic interactions between localized and itinerant spins. The underlying explanation for these effects is the quantum mechanical exchange between localized spins of Mn *d* orbitals and host valence-band *p* orbitals.[1,2] Group III-Mn-V alloys are among the most extensively studied DMSs and a variety of such alloys has been synthesized using different methods. Although there is a general consensus that the ferromagnetic coupling between Mn spins is mediated by itinerant holes, the location of the holes is still a hotly debated issue.[3–7] The original model of ferromagnetism in III-Mn-V alloys was based on the seminal work by Zener[8] and assumed that the holes occupy the valence band and are completely delocalized.[9] This model successfully accounted for several observations and trends. However, there is also a wealth of experimental facts indicating that ferromagnetic coupling can also be found in materials without free holes.[10] An alternative model assumes that in some instances the holes are localized in a narrow Mn impurity band.[4,11–14] Within this framework, higher Mn concentrations and larger bandwidth lead to holes mobile enough to facilitate the exchange interaction between Mn spins.

One of the salient features of the III-Mn-V DMSs is that Mn ions in substitutional Ga sublattice sites not only provide the spin but also act as acceptors, providing holes that lead to metallic conductivity at high concentrations. Previous studies on extrinsic *p* and *n* doping of $Ga_{1-x}Mn_xAs$ thin films have been reported.[15,16] However, the dual contribution of the Mn atoms leads to difficulty in separately controlling spin and hole concentrations, and thus an analysis of the interdependent magnetic and electrical properties of these materials is rather difficult.

In this work, we take advantage of the amphoteric nature of native point defects[17] to systematically control carrier concentrations. In *p*-type $Ga_{1-x}Mn_xAs$, high energy particle irradiation predominantly creates donorlike defects which compensate Mn acceptors and reduce the concentration of holes without altering the concentration of localized Mn spins. We investigate electronic transport and exchange interaction as a function of hole concentration in systems with fixed concentrations of localized magnetic moments by measuring resistivity and magnetization. In addition, to further understand electronic structure, we measure thermopower, which is sensitive to the density of states and the location of the Fermi energy. We provide an analysis of $Ga_{1-x}Mn_xAs$ transport in the framework of mobile holes located in an impurity band described by the band anticrossing (BAC) model,[6] and then we compare our data to both the BAC impurity band model and valence-band transport model.

II. EXPERIMENTAL

A. Native defect controlled carrier concentration

The $Ga_{1-x}Mn_xAs$ samples used in this study were grown by low-temperature molecular beam epitaxy (MBE) and had total (substitutional) Mn contents, x (x_{sub}), of 0.045 (0.036) and 0.038 (0.030) as measured by ion channeling methods.[18] $Ga_{1-x}Mn_xAs$ and GaAs:Be samples were grown using a V/III flux ration of 10 at 250 °C with an As cracker cell, resulting in a growth rate of approximately 2 Å/s. Additional details of the growth are described elsewhere.[19] High concentration GaAs:Zn samples were produced through multiple energy ion implantation of Zn into GaAs followed by rapid thermal annealing. The resulting doped epitaxial films had a flat concentration profile through 120 nm. The $Ga_{1-x}Mn_xAs$ samples were annealed to increase the Curie temperatures to 82 K for the $x=0.045$ and to 84 K for the $x=0.038$ sample.

The intentional damage was produced by Ne^+ ions with energies of 110 and 33 keV to ensure constant damage

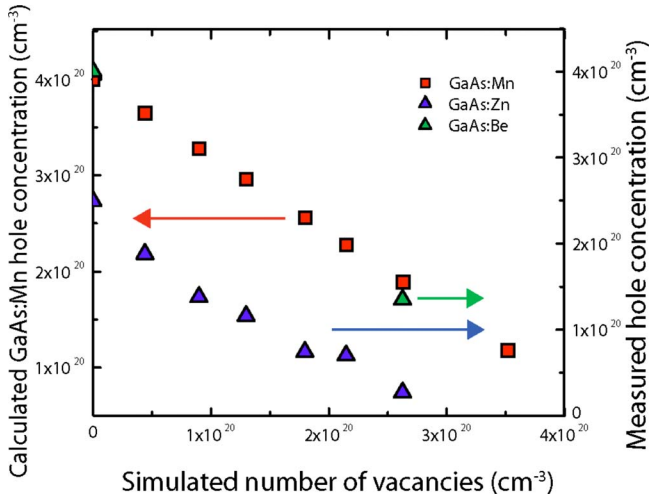

FIG. 1. (Color online) Carrier concentration as a function of vacancy concentration generated by irradiation. $Ga_{1-x}Mn_xAs$ concentration (red squares) is calculated by combining initial ECV measurements with the carrier removal rate monitored by Hall effect in the GaAs:Zn and GaAs:Be samples (triangles).

through 150-nm-thick films. The dose at each energy was systematically incremented in steps of 5×10^{11} and 1×10^{11} cm^{-2}, respectively, to increase the damage and reduce the hole concentration. The initial hole concentrations of 4×10^{20} cm^{-3} (x=0.045) and 6×10^{20} cm^{-3} (x=0.038) were determined using electrochemical capacitance voltage (ECV) profiling.[20] However, due to electrochemical-surface interactions in damaged samples, this technique was unreliable for heavily implanted films. Since the anomalous Hall effect prevents conventional carrier concentration measurements on $Ga_{1-x}Mn_xAs$,[1] the carrier removal rate was determined with Hall effect measurements in heavily doped GaAs:Zn ($p=2\times10^{20}$ cm^{-3}) and GaAs:Be ($p=4\times10^{20}$ cm^{-3}) samples irradiated the same way as $Ga_{1-x}Mn_xAs$.

Native defects in semiconductors are typically charged and thus act as dopants. Therefore, the intentional introduction of native defects in the host lattice through irradiation can be used to change the concentration of mobile charge carriers without affecting the concentration or site locations of dopants in an already existing sample.[21] According to the amphoteric defect model (ADM), the character (donor or acceptor) of the native defects depends on the location of the Fermi energy (E_F) relative to a fixed energy reference, the Fermi stabilization energy (E_{FS}).[17,22] The damage-induced reduction of the hole concentration in our p-type samples is a manifestation of the fact that E_F in p-type GaAs is located well below E_{FS} and thus donors (V_{As}^{3+}) are the dominant defects produced by high energy particle irradiation.

Figure 1 shows the carrier concentrations for a $Ga_{1-x}Mn_xAs$ sample and the GaAs:Zn sample as a function of the concentration of vacancies calculated using the SRIM 2008 software (stopping and range of ions in matter).[23] The concentration of vacancies provides a standardized measure of damage that is proportional to the implantation dose and allows direct comparison of damage produced by combinations of different ion species, energies, and doses. As is seen in Fig. 1, the hole concentration in the samples doped with hydrogenic acceptors decreases linearly with increasing vacancy concentration corresponding to a constant hole removal rate of 0.91 hole/vacancy. Using ion irradiation, we were able to reduce the hole concentration in wide concentration ranges from 4×10^{20} to 1.3×10^{20} cm^{-3} in $Ga_{0.955}Mn_{0.045}As$ and from 6×10^{20} to 3.5×10^{19} cm^{-3} in $Ga_{0.962}Mn_{0.038}As$. We note that, although the irradiated ion (Ne^+) is inert, the highest Ne concentration in each sample is two orders of magnitude lower than the Mn concentration and should not affect the hole concentration either through doping or significant displacement of the dopant atoms.

B. Electrical and magnetic properties

The temperature dependent magnetization in samples with different hole concentrations has been measured using a standard superconducting quantum interference device magnetometer at an applied field of 50 Oe parallel to a ⟨110⟩ direction on a sample with x_{sub}=0.036. The data shown in Fig. 2(a) indicate an overall decrease in the maximum value of magnetization and the Curie temperature (T_C) with decreasing hole concentration. The saturation moment per substitutional Mn atom (at 5 K) and T_C are reduced from 4.37μ_B and 85 K in the as-grown annealed sample to 1.66μ_B and 46 K in the heaviest irradiated sample, respectively (here, "as grown" refers to a sample that has not been irradiated). T_C vs hole concentration is plotted in Fig. 2(b) to emphasize the understandable decrease in T_C in response to a reduced hole concentration. Similarly, the decrease in the saturation magnetization is consistent with a picture where the Mn doping is held constant, but some Mn are rendered ferromagnetically inactive due to the reduced coupling from fewer carriers.

Electrical transport measurements were performed in the van der Pauw configuration using Ohmic pressed In contacts. Variable temperature resistivity measurements are shown as a function of temperature in Fig. 3(a). The annealed reference sample exhibits electrical transport characteristics typical for metallic $Ga_{1-x}Mn_xAs$ including critical behavior near T_C.[24,25] As the irradiation dose is increased, the peak near T_C fades and the sample undergoes a metal-insulator transition.

We use the hole removal rate to determine the hole concentration as a function of irradiation dose in $Ga_{1-x}Mn_xAs$, then extracted the mobility from

$$\mu = (ep\rho)^{-1}, \tag{1}$$

where e is the charge of the carrier, p is the concentration of holes, and ρ is the sample resistivity. Figure 3(b) compares the hole mobilities in $Ga_{1-x}Mn_xAs$ to those measured in GaAs doped with the conventional hydrogenic acceptors Zn and Be. The shown theoretical fits will be explained below. Clearly the mobility in $Ga_{1-x}Mn_xAs$ is significantly smaller than the mobility in GaAs doped with Be or Zn for similar hole concentrations. This result agrees with a previous report,[6] which showed that the holes in $Ga_{1-x}Mn_xAs$ are located in a narrow Mn impurity band but are completely delocalized in GaAs doped with standard acceptors such as Be or Zn.

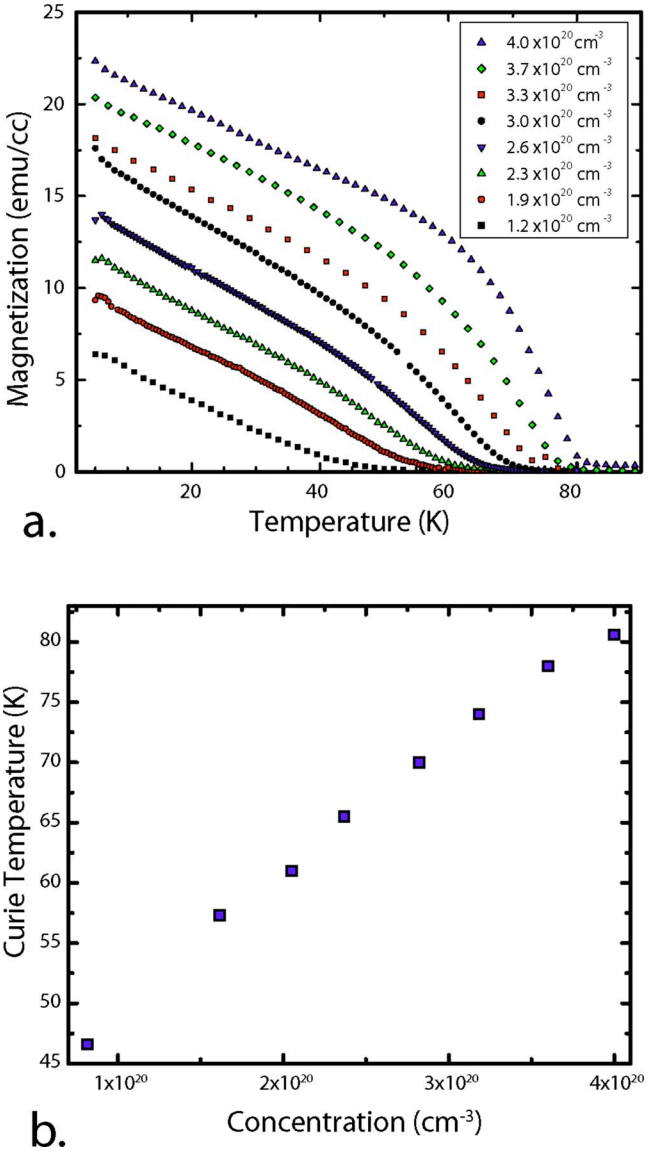

FIG. 2. (Color online) (a) Magnetization as a function of temperature for a series of irradiated $Ga_{0.955}Mn_{0.045}As$. (b) Curie temperature for each sample as a function of hole concentration.

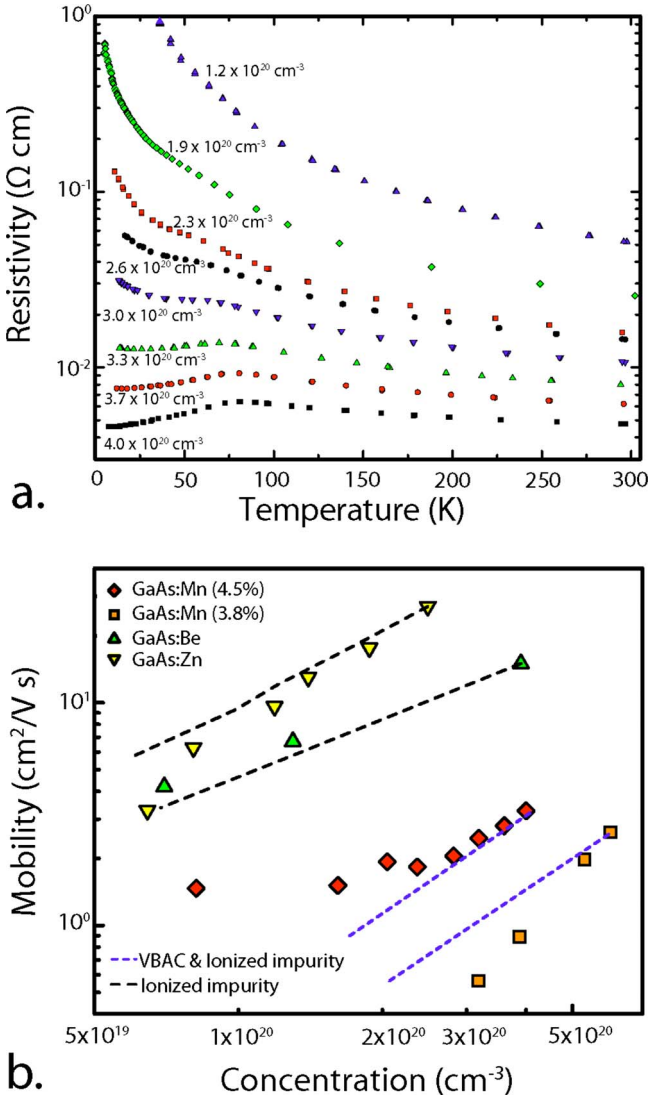

FIG. 3. (Color online) (a) Resistivity as a function of temperature of irradiated $Ga_{0.955}Mn_{0.045}As$. (b) Room temperature (300 K) mobility as a function of concentration for two samples of $Ga_{1-x}Mn_xAs$ and Hall effect-measured mobility for nonmagnetic GaAs:Be and GaAs:Zn samples. Fits (dashed lines) are based on the ionized impurity model; the blue dashed lines (shorter dashes) use an effective mass derived from VBAC, while the black dashed lines represent calculations based on valence-band transport.

Finally, we measured thermopower in the sample with $x_{sub}=0.030$ as a function of temperature for different hole concentrations. These data are the expected order of magnitude for $Ga_{1-x}Mn_xAs$ (Ref. 26) and are displayed in Fig. 4(a). The dark lines in Fig. 4(a) represent calculations based on the theory discussed below. The thermopower apparatus has been described elsewhere.[27,28]

III. ELECTRONIC BAND STRUCTURE CALCULATIONS

The complex nature of the sixfold degenerate valence band makes any quantitative analysis of the electronic and magnetic properties of III-Mn-V semiconductors rather difficult. In the free hole model, the electronic structure of these materials is typically approximated by the valence structure of the host III-V semiconductor, in which case the Mn impurities are only a source of free holes and localized spins. This greatly simplifies the problem and allows for semiquantitative evaluations of some of the properties of these materials. In contrast, in the impurity band model, incorporation of Mn acceptors drastically affects the electronic structure of the host matrix, but there is presently no accepted model of the evolution of the impurity band structure with increasing Mn content. It has been shown more than ten years ago that the interaction of localized impurity states with extended band states can be described by the BAC model.[29] The model has been successfully used to analyze the interaction of localized isovalent impurity states with the conduction band[30,31] as well as with the valence band.[32] Recently the valence-band anticrossing (VBAC) model has been used to describe the electronic structure of $Ga_{1-x}Mn_xAs$.[6]

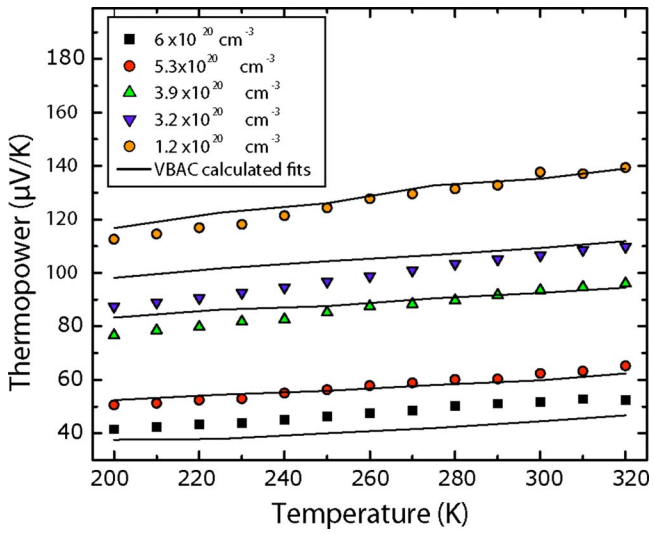

FIG. 4. (Color online) Thermopower as a function of temperature of irradiated $Ga_{1-x}Mn_xAs$. Colored points indicate measured data while solid lines are fits based on the VBAC model.

A. Mobility

We fit our data using a mobility model applicable to high carrier concentration samples. This analysis establishes a specific trend in sample mobility, allowing a comparison between $Ga_{1-x}Mn_xAs$ samples and GaAs containing more traditional dopants. We use a standard relaxation time approach to analyze the concentration dependence of the hole mobility. Because of the large hole concentrations in our samples, it is reasonable to assume that the ionized impurities are the dominant scattering centers. Within this framework, the overall mobility obeys the equation[33]

$$\mu = \frac{\tau(E)}{m^*(E)}, \tag{2}$$

where $m^*(E)$ is the effective mass and $\tau(E)$ is the energy-dependent scattering time, which is calculated according to a standard form for ionized impurity scattering,

$$\frac{1}{\tau} = \frac{2.415 N_{\mathrm{II}} m^{*-1/2} \left(\frac{E}{k_b}\right)^{-3/2}}{\varepsilon^2} \ln\left[(1+\xi) - \left(\frac{\xi}{(1+\xi)}\right)\right]. \tag{3}$$

Here N_{II} is the number of ionized impurities and

$$\xi = \frac{4}{a}\left(\frac{E}{k_b T}\right), \tag{4}$$

where a is the reduced screening energy with screening length l_D,[33]

$$a = \frac{\hbar^2}{2m^* l_D k_b T}. \tag{5}$$

In general, a calculation of the average macroscopic mobility requires integration over the energy, E. However, for the degenerate hole case when the Fermi level is in a band, the mobility can be approximated by the mobility at the Fermi energy, E_F. This approximation works well for the Be- and Zn-doped samples in which the Fermi energy is in the valence band for concentrations higher than 10^{19} cm^{-3}. However, as will be shown later, this mobility model based on ionized impurity scattering applies only to the $Ga_{1-x}Mn_xAs$ samples with the highest hole concentrations where the Fermi level is in the Mn impurity band in $Ga_{1-x}Mn_xAs$. Based on these degenerate statistics, the mobility model is identical for both valence band and impurity band transport, with the exception of the value used for the effective hole mass. In the case of valence-band transport, we assume a parabolic valence band with hole effective mass of $m_h = 0.45m_0$. In the impurity band framework, the effective mass at the Fermi vector, $k_F = (3\pi^2 p)^{1/3}$, is calculated from the dispersion relations derived from a 12×12 Hamiltonian matrix for the VBAC model.[6,32]

The fixed initial concentration of ionized impurities, $N_{\mathrm{II\text{-}0}}$, is the only empirical parameter used in the model and is determined by fitting the mobility of the as-grown samples. According to the ADM,[17] triply charged ($Z=3$) vacancylike donor defects are responsible for hole compensation in irradiated p-GaAs. Therefore the hole concentration in irradiated samples is given by $p = p_0 - ZN_d$, where p_0 is the hole concentration in as-grown samples. Here N_d is the concentration of irradiation-produced triply charged donor defects which scatter according to Coulombic interaction. As a result, the effective concentration of ionized scattering centers in irradiated samples is given by $N_{\mathrm{II}} = N_{\mathrm{II\text{-}0}} + Z^2 N_d$.

As shown in Fig. 3(b), the hole mobilities in the as-grown samples are 2.6 $cm^2/V\,s$ for the $Ga_{0.962}Mn_{0.038}As$ sample and 3.3 $cm^2/V\,s$ for the $Ga_{0.955}Mn_{0.045}As$ sample. Both of these measurements are consistent with previously reported hole mobilities in $Ga_{1-x}Mn_xAs$ and one order of magnitude lower than measured values for holes in GaAs doped with impurities other than Mn. This large difference in hole mobilities cannot be explained by spin-disorder scattering which is proportional to magnetic susceptibility and therefore should depend strongly on temperature. In metallic $Ga_{1-x}Mn_xAs$, zero-field resistivity is very weakly dependent on the temperature suggesting that spin disorder cannot be the dominant mechanism limiting the mobility.[6] Instead, the low hole mobilities can be explained with VBAC assuming an as-grown ionized impurity concentration $N_{\mathrm{II\text{-}0}}$ equal to 1.6×10^{21} cm^{-3} in the first sample and 1.1×10^{21} cm^{-3} in the second sample. Although high, these concentrations are approximately 5% of all the lattice sites in the highly defective film and follow the relationship observed by Alberi *et al.* of $N_{\mathrm{II\text{-}0}} = 2.5p$.[6] The dashed blue lines in Fig. 3(b) represent the extension of the VBAC ionized impurity model to lower concentrations as described above and show good agreement with the irradiated films, diverging only at low carrier concentrations when, as will be shown later, the Fermi level no longer lies in the impurity band.

Alternatively, an attempt to explain these low mobilities in $Ga_{1-x}Mn_xAs$ using the free hole model and standard GaAs effective hole mass requires an unrealistically high initial ionized impurity concentration of 1.2×10^{22} cm^{-3}, which is equivalent to ionized defects present in more than half of all GaAs lattice sites. In contrast, the valence-band model explains quite well the concentration dependence of the hole mobility in GaAs:Zn and GaAs:Be. The black dashed lines in

Fig. 3(b) represent an ionized impurity calculation assuming triply charged ionized impurity concentrations of 1.1×10^{21} and 2.8×10^{21} cm^{-3} for highly doped as-grown Zn- and Be-doped samples, respectively. The calculations account very well for the dependence of the mobility on the concentration of holes. The above results demonstrate that there is a clear difference in both the magnitude and the dependence of hole concentration of the mobilities in GaAs doped with hydrogenic acceptors compared to $Ga_{1-x}Mn_xAs$, indicating a different nature of the mobile holes in these two types of materials.

B. Thermopower

In order to analyze the thermopower of our samples as a function of concentration, we adopt a simple form of VBAC that encompasses the main features of the band anticrossing without the complexity of the multifold degenerate valence band. In this approximation the dispersion relations are given by a simple expression[29]

$$E_{\pm}(k) = \tfrac{1}{2}[E_{\mathrm{Mn}} + E(k)] \pm \sqrt{[E(k) - E_{\mathrm{Mn}}]^2 + 4C^2x}, \quad (6)$$

where in this case $E_-(k)$ represents the upper subband which is mostly impuritylike, $E_+(k)$ represents the lower subband which has more valence-band character, E_{Mn} is the energy of the Mn dopant relative to the valence-band maximum ($E_{\mathrm{Mn}}=110$ meV), C is an empirical coupling constant, 0.39, for the $Ga_{1-x}Mn_xAs$ system,[6] and x gives the sample composition.

The corresponding wave functions are a combination of the wave function of the delocalized valence-band states, $|B\rangle$, and the wave function of highly localized Mn acceptors, $|\mathrm{Mn}\rangle$,

$$|\psi_+\rangle = -\sin\left(\frac{\theta}{2}\right)|B\rangle + \cos\left(\frac{\theta}{2}\right)|\mathrm{Mn}\rangle, \quad (7)$$

$$|\psi_-\rangle = \sin\left(\frac{\theta}{2}\right)|\mathrm{Mn}\rangle + \cos\left(\frac{\theta}{2}\right)|B\rangle, \quad (8)$$

where

$$\theta(k) = \tan^{-1}\left(\frac{2Cx^{1/2}}{E(k) - E_{\mathrm{Mn}}}\right). \quad (9)$$

The density of states can be derived from the dispersion relations in Eq. (6). For the impurity band [hole energies between $E_-(0)$ and the acceptor level of Mn (E_{Mn})], the density of states has the form

$$g_-(E) = \frac{\sqrt{2}(m^*)^{3/2}}{\pi^2\hbar^3}\frac{[(E_{\mathrm{Mn}} - E)^2 + C^2x][E(E_{\mathrm{Mn}} - E) + C^2x]^{1/2}}{(E_{\mathrm{Mn}} - E)^{5/2}}. \quad (10)$$

The nature of the impurity band states strongly depends on energy separation from the Mn level. It gradually changes from fully localized at $E=E_{\mathrm{Mn}}$ to mostly delocalized for $E(k=0)$. Similarly, the states at the top of the valence band after anticrossing are mostly localized, while states deep in the band are predominantly delocalized. Therefore the total

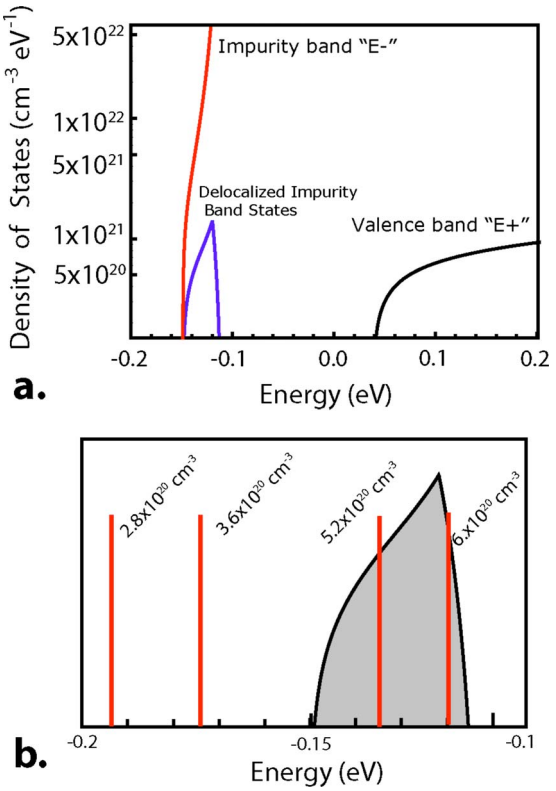

FIG. 5. (Color online) (a) Approximated density of states used in transport calculations with reference to the original GaAs valence band. Blue line represents delocalized states of the original impurity band (red line). (b) Close-up image of the impurity band [same energy scale as (a), arbitrary units on y axis] with the Fermi level denoted in terms of concentration for selected samples of the $x=0.038$ irradiated series.

density of states in the impurity band can be divided in the delocalized and localized states, with each density of states given by

$$g_{del}(E) = \left(-\sin\left\{\frac{\theta[k(E)]}{2}\right\}\right)^2 g_-(E), \quad (11)$$

$$g_{loc}(E) = \cos\left\{\frac{\theta[k(E)]}{2}\right\}^2 g_-(E), \quad (12)$$

respectively. In the following we assume that only delocalized states of both the impurity band and the valence band contribute to the charge transport. This portion of the impurity band with relation to the VBAC density of states is pictured in Fig. 5(a).

Finally, with such a significant addition of Mn to the sample by the process of low-temperature MBE, the sample is inhomogeneous in composition. Physically, this means that the impurity band has band tails and is generally variable across the sample. We reflect this sample imperfection through a standard Lorentzian broadening according to

$$g_{del\text{-}broad}(E') = \int g_{del}(E) \times \frac{(\Gamma/\pi)}{\Gamma^2 + (E - E')^2} dE, \quad (13)$$

where Γ is a broadening parameter between 10 and 50 meV. Thus, the final density of states takes into account the anticrossing interaction, delocalization of states, and realistic composition fluctuations in our samples.

We then apply the VBAC model to analyze our thermopower measurements. Thermopower is a function of the Fermi level position with respect to the density of states and therefore irradiation-induced changes in thermopower reflect the movement of the Fermi level relative to the impurity band. Figure 5(b) shows the impurity band density of states as a function of energy along with the calculated Fermi level for each sample concentration. For hole concentrations below 1×10^{20} cm^{-3}, the large majority of holes have been compensated by vacancies and roughly 3% of the lattice is occupied by defect sites; thus we believe that the VBAC band structure may no longer be intact due to additional impurity band formation or carrier concentration saturation according to the ADM. Therefore, we only consider these concentrations that have Fermi levels within 0.1 eV (the width of the impurity band) of the impurity band.

For modeling, we consider two possible contributions to the thermopower: diffusion and exchange due to the paramagnetic nature of the sample.[34] The calculated density of states can be directly applied in the expression for diffusion thermopower,

$$S_{diffusion} = \frac{\int (E - E_f) \frac{dF(E)}{dE} g_{del}(E) dE}{eT \int \frac{dF(E)}{dE} g(E)_{del} dE}, \quad (14)$$

where $g_{del}(E)$ is the delocalized density of states and $F(E)$ is the Fermi-Dirac distribution function. In DMSs, one expects additional contribution to the thermopower originating from the exchange interaction.[35] According to Kondo's derivation,[34] the exchange thermopower can be expressed as

$$S_{exchange} = S_0 \frac{T}{T + T_0}, \quad (15)$$

where T_0 is the Kondo temperature and S_0 is a temperature-independent parameter defined in terms of the exchange integral, spin operator, resistivity, potential, and physical constants. It has been shown that T_0 is on the order of 10 K in $Ga_{1-x}Mn_xAs$ films[36] and thus taken to be negligible at the high temperatures that include our range of measurements. Consequently the exchange contribution can be approximated by a temperature-independent constant S_0.[35] The only empirical parameters employed for the fit are the small contribution from S_0 and the broadening parameter to account for realistic composition fluctuations.

The results of calculations of thermopower as a function of carrier concentration are shown in Fig. 6 along with thermopower data for $Ga_{1-x}Mn_xAs$ and GaAs:Be. Similar to the mobility case, the best fit for the $Ga_{1-x}Mn_xAs$ data comes from the VBAC model with a small temperature- and concentration-independent contribution from the inclusion of the exchange thermopower ($S = S_{diffusion} + S_{exchange}$). Here we empirically find S_0 to be 20 μV/K, which is only a small (13%) contribution to the modeled fit. It is worth noting that, even without the Kondo contribution, the VBAC model very well reproduces the convex shape of the thermopower dependence on the hole concentration as well as its high numerical values. This is in stark contrast to the behavior predicted by a model based on hydrogenically doped GaAs with valence-band transport where, as is seen in Fig. 6, the thermopower is significantly lower and has concave behavior. The concave dependence is in good agreement with calculations that assume that the thermopower is solely determined by free valence-band holes.

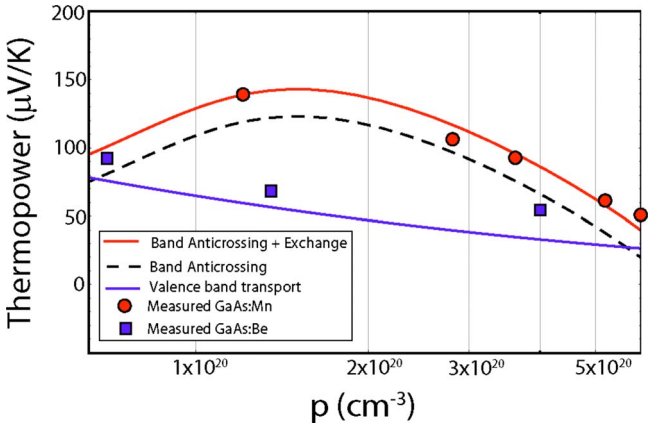

FIG. 6. (Color online) Thermopower as a function of concentration. Circles indicate measured data for $Ga_{1-x}Mn_xAs$ samples, while squares show GaAs:Be data. The solid red line (convex) shows the calculation developed from both exchange and diffusion thermopower based on valence-band anticrossing, while the dashed curve shows only the anticrossing calculation without the empirically determined exchange contribution. The blue line shows a thermopower calculation for a system with valence-band transport.

To further explore the electronic structure, we have also calculated the temperature dependence of the thermopower for the samples with different hole concentrations. As indicated in Fig. 4, the VBAC fits agree well with the experimental data over a wide range of temperatures. It should be noted that we have used the same fitting parameters as in the room temperature calculations. Compared to the free hole model, the VBAC model provides a more realistic trend for $Ga_{1-x}Mn_xAs$ thermopower data as a function of both hole concentration and temperature.

IV. DISCUSSION

Our analysis of the hole-concentration-dependent transport properties of $Ga_{1-x}Mn_xAs$ strongly supports the model in which mobile holes are located in the Mn impurity band. The results clearly show distinct quantitative and qualitative differences in hole concentration dependence of the mobility and thermopower in $Ga_{1-x}Mn_xAs$ and GaAs doped with Be or Zn. The key difference between those two materials is the acceptor binding energy: about 24 meV for shallow hydrogenic acceptors such as Be or Zn and 110 meV for Mn. The

difference in the binding energy has important consequences for impurity band evolution with increasing acceptor concentration. In the case of shallow acceptors, the relatively large size of the acceptor wave function leads to significant overlap of the wave functions with the adjacent acceptor sites and results in a metal-to-insulator transition and formation of an impurity band that merges into the valence band at relatively low acceptor concentrations. A weak band anticrossing interaction does not play a significant role in this case. Therefore the transport properties of GaAs doped with either Be or Zn are well described by free holes in the valence band. In contrast, for the more localized and deeper Mn acceptors in $Ga_{1-x}Mn_xAs$, the band anticrossing interaction is stronger and dominates the weaker electrostatic interaction. Thus the impurity band remains separated from the valence band at any impurity concentration. We show that the VBAC offers a good explanation of the hole transport properties in this case.

Further support for the impurity band model is provided by the hole-concentration-dependent magnetic properties of $Ga_{1-x}Mn_xAs$. As is seen in Fig. 2, decreasing the hole concentration decreases both T_C and the magnetic moment. Nevertheless, a relatively high T_C of more than 40 K is found in samples with very high resistivity (Fig. 3). The observed behaviors can be understood within the framework of the ADM in conjunction with VBAC. The irradiation-produced donors are uniformly distributed throughout the sample, and as the Fermi level moves toward E_{FS} with increasing irradiation dose, electrons fill the impurity band. However, significant spatial fluctuations of the Mn concentration typically exist in as-grown $Ga_{1-x}Mn_xAs$. Therefore, for high enough irradiation dose, the sample will be divided into low Mn content, nonconducting regions with fully filled impurity band, and higher Mn content regions that remain incompletely compensated with holes in the impurity band. The magnetic properties are then determined by the sum of the contributions from these regions with different ferromagnetic couplings and different Curie temperatures. This will eventually lead to a reduction of the total magnetic moment. Similar "two region" arguments were used to explain the reduction in saturation magnetization with alloying in $Ga_{1-x}Mn_xAs_{1-y}P_y$.[7] The increase of the nonconducting fraction of the sample volume accounts well for the increase of the sample resistance with increasing irradiation dose.

In parallel, we observe that changing the hole concentration has a profound effect on the shape of the thermomagnetic profiles. While magnetic anisotropy is not specifically addressed in the VBAC model, we note that our model is not inconsistent with the concept of anisotropy since we take into account the spin-orbit coupling of the carriers, which is generally believed to be the origin of magnetic anisotropy in Mn-doped III-V ferromagnetic semiconductors.[37] Changes in the shape of the temperature dependence of the magnetization $M(T)$ were analyzed theoretically by Das Sarma and co-workers[38,39] using an impurity band model. According to this model, the temperature profile of $M(T)$ curves changes from convex to concave with increasing compensation ratio. This is in clear qualitative agreement with our data as the compensation ratio is increasing with the increase of the donor concentration occurring as a result of increasing irradiation dose. It should be noted that we cannot discount the

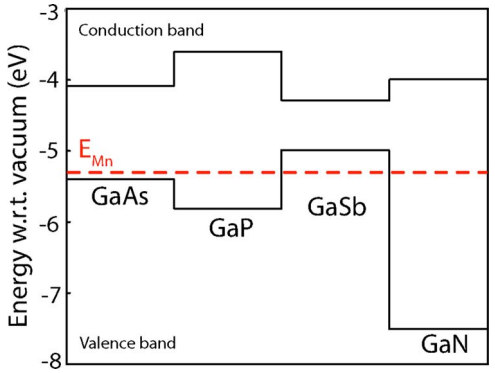

FIG. 7. (Color online) Mn acceptor level (red dashed line) with respect to III-V semiconductor band edges.

effect of carrier-concentration-dependent magnetic anisotropy, which is known in both $Ga_{1-x}Mn_xAs$ and $Ga_{1-x}Mn_xP$ to affect the anisotropy between in-plane ⟨110⟩ directions.[40,41] However, both the magnetically hard and easy ⟨110⟩ in-plane directions exhibit the same changes in line shape with compensation. This is consistent with previous results in $Ga_{1-x}Mn_xP$ and $Ga_{1-x}Mn_xAs_{1-y}P_y$ which showed an empirical connection between moving through the metal-insulator transition and the shape of the $M(T)$ profiles.[7]

Although our considerations were limited to $Ga_{1-x}Mn_xAs$, the band anticrossing model can be applied to other group III-Mn-V DMSs. The location of the Mn acceptor level, about 0.11 eV above the valence band, is a unique aspect of $Ga_{1-x}Mn_xAs$. This binding energy, more than four times larger than the hydrogenic acceptor level, is large enough to assure good localization of bound hole states but, on the other hand, is small enough to result in a strong anticrossing interaction with the valence band. Formation of the impurity band well separated from the valence band but wide enough to have relatively mobile holes appears to be a key feature responsible for the high T_C in $Ga_{1-x}Mn_xAs$.

Figure 7 shows the location of the Mn acceptor level relative to the valence band of several different III-V semiconductors. A much weaker anticrossing interaction is expected in $Ga_{1-x}Mn_xP$ where the highly localized Mn level lies nearly 400 meV above the valence-band edge. As a result, $Ga_{1-x}Mn_xP$ exhibits high resistance with hoppinglike conductivity.[7,10] However even in this case the holes in the impurity band are able to facilitate the ferromagnetic coupling between Mn spins, resulting in a moderately high Curie temperature of 60 K for $x=0.042$.[10]

On the opposite end of the spectrum, as shown in Fig. 7, the Mn level in GaSb is located at about 0.3 eV below the valence-band edge. Consequently, Mn is a shallow hydrogenic acceptor with holes bound by the Coulomb potential. In this case, the delocalized Mn states form a band that, at high Mn concentrations, merges with the valence band in a manner similar to hydrogenic acceptors. The valence-band holes are therefore responsible for the ferromagnetic coupling. Indeed, reported mobilities for high concentrations ($\sim 8\times 10^{20}$ cm^{-3}) of *both* GaSb doped with traditional dopants and GaSb doped with up to 14% Mn are on the order of 200 $cm^2/V\,s$ and in agreement with Mn behaving as a hydrogenic dopant in GaSb.[42,43] In fact, $Ga_{1-x}Mn_xSb$ and

$In_{1-x}Mn_xSb$ with their relatively low T_C's are the materials closest to the model system satisfying the conditions for application of the Zener-like model of ferromagnetic coupling in semiconductors.[9]

V. CONCLUSIONS

We have shown that intentionally introduced native defects can be used to control the free hole concentration in DMSs. Using high energy particle irradiation, we have carried out a systematic study of the hole-concentration-dependent properties of $Ga_{1-x}Mn_xAs$. The results of the measurements of the electron mobility and thermopower of this system can be understood by only assuming that the mobile holes responsible for the charge transport and magnetic properties reside in a Mn derived impurity band. The main features of the observed hole transport can be explained by the valence-band anticrossing model that is used to describe the electronic structure of the Mn impurity band. The results have important consequences for understanding of the ferromagnetic coupling in all group III-Mn-V DMSs and provide guidance for optimization of the material properties for spintronic applications.

ACKNOWLEDGMENTS

We would like to thank Jeff Beeman at LBNL for several irradiations. This work was supported by the Director, Office of Science, Office of Basic Energy Sciences, Division of Materials Sciences and Engineering, of the (U.S.) Department of Energy under Contract No. DE-AC02-05CH11231. M.A.M. and N.M. thank the Department of Defense for NDSEG support and P.R.S. thanks the National Science Foundation for support.

[1] F. Matsukura, H. Ohno, A. Shen, and Y. Sugawara, Phys. Rev. B **57**, R2037 (1998).
[2] J. K. Furdyna, J. Appl. Phys. **64**, R29 (1988).
[3] T. Jungwirth, J. Sinova, A. H. MacDonald, B. L. Gallagher, V. Novák, K. W. Edmonds, A. W. Rushforth, R. P. Campion, C. T. Foxon, L. Eaves, E. Olejník, J. Mašek, S.-R. Eric Yang, J. Wunderlich, C. Gould, L. W. Molenkamp, T. Dietl, and H. Ohno, Phys. Rev. B **76**, 125206 (2007).
[4] K. S. Burch, D. B. Shrekenhamer, E. J. Singley, J. Stephens, B. L. Sheu, R. K. Kawakami, P. Schiffer, N. Samarth, D. D. Awschalom, and D. N. Basov, Phys. Rev. Lett. **97**, 087208 (2006).
[5] M. E. Flatte, IEEE Trans. Electron Devices **54**, 907 (2007).
[6] K. Alberi, K. M. Yu, P. R. Stone, O. D. Dubon, W. Walukiewicz, T. Wojtowicz, X. Liu, and J. K. Furdyna, Phys. Rev. B **78**, 075201 (2008).
[7] P. R. Stone, K. Alberi, S. K. Z. Tardif, J. W. Beeman, K. M. Yu, W. Walukiewicz, and O. D. Dubon, Phys. Rev. Lett. **101**, 087203 (2008).
[8] C. Zener, Phys. Rev. **81**, 440 (1951); **83**, 299 (1951).
[9] T. Dietl, H. Ohno, F. Matsukura, J. Cibert, and D. Ferrand, Science **287**, 1019 (2000).
[10] For example, M. A. Scarpulla, B. L. Cardozo, R. Farshchi, W. M. Hlaing Oo, M. D. McCluskey, K. M. Yu, and O. D. Dubon, Phys. Rev. Lett. **95**, 207204 (2005).
[11] J. Okabayashi, A. Kimora, O. Rader, T. Mizokawa, A. Fujimori, T. Hayashi, and M. Tanaka, Physica E (Amsterdam) **10**, 192 (2001).
[12] B. L. Sheu, R. C. Myers, J.-M. Tang, N. Samarth, D. D. Awschalom, P. Schiffer, and M. E. Flatte, Phys. Rev. Lett. **99**, 227205 (2007).
[13] J.-M. Tang and M. E. Flatte, Phys. Rev. Lett. **101**, 157203 (2008).
[14] L. P. Rokhinson, Y. Lyanda-Geller, Z. Ge, S. Shen, X. Liu, M. Dobrowolska, and J. K. Furdyna, Phys. Rev. B **76**, 161201(R) (2007).
[15] K. M. Yu, W. Walukiewicz, T. Wojtowicz, W. L. Lim, X. Liu, U. Bindley, M. Dobrowolska, and J. K. Furdyna, Phys. Rev. B **68**, 041308(R) (2003).
[16] Y. J. Cho, K. M. Yu, X. Liu, W. Walukiewicz, and J. K. Furdyna, Appl. Phys. Lett. **93**, 262505 (2008).
[17] W. Walukiewicz, Appl. Phys. Lett. **54**, 2094 (1989).
[18] K. M. Yu, W. Walukiewicz, T. Wojtowicz, I. Kuryliszyn, X. Liu, Y. Sasaki, and J. K. Furdyna, Phys. Rev. B **65**, 201303(R) (2002).
[19] X. Liu, Y. Sasaki, and J. K. Furdyna, Phys. Rev. B **67**, 205204 (2003).
[20] K. M. Yu, W. Walukiewicz, T. Wojtowicz, W. L. Lim, X. Liu, Y. Sasaki, M. Dobrowolska, and J. K. Furdyna, Appl. Phys. Lett. **81**, 844 (2002).
[21] For example, S. X. Li, K. M. Yu, J. Wu, R. E. Jones, W. Walukiewicz, J. W. Ager III, W. Shan, E. E. Haller, H. Lu, and W. J. Schaff, Phys. Rev. B **71**, 161201(R) (2005).
[22] W. Walukiewicz, Phys. Rev. B **37**, 4760 (1988).
[23] SRIM 2008, http://www.srim.org
[24] H. Ohno, J. Magn. Magn. Mater. **200**, 110 (1999).
[25] V. Novak, K. Olejník, J. Wunderlich, M. Cukr, K. Výborný, A. W. Rushforth, K. W. Edmonds, R. P. Campion, B. L. Gallagher, Jairo Sinova, and T. Jungwirth, Phys. Rev. Lett. **101**, 077201 (2008).
[26] Y. Pu, E. Johnston-Halperin, D. D. Awschalom, and Jing Shi, Phys. Rev. Lett. **97**, 036601 (2006).
[27] J. W. Ager III, N. Miller, R. E. Jones, K. M. Yu, J. Wu, W. J. Schaff, and W. Walukiewicz, Phys. Status Solidi B **245**, 873 (2008).
[28] M. S. Brandt, P. Herbst, H. Angerer, O. Ambacher, and M. Stutzmann, Phys. Rev. B **58**, 7786 (1998).
[29] W. Shan, W. Walukiewicz, J. W. Ager III, E. E. Haller, J. F. Geisz, D. J. Friedman, J. M. Olson, and S. R. Kurtz, Phys. Rev. Lett. **82**, 1221 (1999).
[30] W. Walukiewicz, W. Shan, K. M. Yu, J. W. Ager III, E. E. Haller, I. Miotkowski, M. J. Seong, H. Alawadhi, and A. K. Ramdas, Phys. Rev. Lett. **85**, 1552 (2000).
[31] J. Wu, W. Shan, and W. Walukiewicz, Semicond. Sci. Technol. **17**, 860 (2002).
[32] K. Alberi, J. Wu, W. Walukiewicz, K. M. Yu, O. D. Dubon, S. P.

Watkins, C. X. Wang, X. Liu, Y.-J. Cho, and J. K. Furdyna, Phys. Rev. B **75**, 045203 (2007).
[33] W. Walukiewicz, L. Lagowski, L. Jastrzebski, M. Lichtensteiger, and H. C. Gatos, J. Appl. Phys. **50**, 899 (1979).
[34] J. Kondo, Solid State Phys. **23**, 183 (1970).
[35] V. Osinniy, K. Dybko, A. Jedrzejczak, M. Arciszewska, W. Dobrowolski, T. Story, M. V. Radchenko, V. Sichkovskiy, G. Lashkarev, S. Olsthoorn, and J. Sadowski, arXiv:cond-mat/0409659 (unpublished).
[36] H. T. He, C. L. Yang, W. K. Ge, J. N. Wang, X. Dai, and Y. Q. Wang, Appl. Phys. Lett. **87**, 162506 (2005).
[37] T. Dietl, H. Ohno, and F. Matsukura, Phys. Rev. B **63**, 195205 (2001).
[38] S. Das Sarma, E. H. Hwang, and A. Kaminski, Phys. Rev. B **67**, 155201 (2003).
[39] A. Kaminski and S. Das Sarma, Phys. Rev. Lett. **88**, 247202 (2002).
[40] M. Sawicki, F. Matsukura, A. Idziaszek, T. Dietl, G. M. Schott, C. Ruester, C. Gould, G. Karczewski, G. Schmidt, and L. W. Molenkamp, Phys. Rev. B **70**, 245325 (2004).
[41] P. R. Stone, C. Bihler, M. Kraus, M. A. Scarpulla, J. W. Beeman, K. M. Yu, M. S. Brandt, and O. D. Dubon, Phys. Rev. B **78**, 214421 (2008).
[42] O. Madelung, U. Rössler, and M. Schulz, *Condensed Matter: Group IV Elements, IV-IV and III-V Compounds*, Landolt-Börnstein, New Series, Group III, Vol. 41A1b, Pt. B (Springer-Verlag, Berlin, 2002), p. 1622.
[43] T. Adhikari and S. Basu, Jpn. J. Appl. Phys., Part 1 **33**, 4581 (1994).